2

Methodology

A combined experimental and theoretical approach has proved to be a useful tool to study the spectroscopy of molecules. This Chapter presents a concise description of the various experimental techniques like FTIR, FT-Raman and UV-Vis spectroscopy along with the quantum chemical methods like *ab initio* HF, DFT and MP2, which are used in the present study. Additional specific details for each studied molecule will be presented in the relevant Chapters .

2.1 Experimental techniques

2.1.1 FTIR spectroscopy

Infrared spectroscopy probes the molecular vibrations in great detail and contributes considerably not only to identification of the molecules but also to study the molecular structure. Furthermore, an interaction with the surrounding environment also causes a change in molecular vibrations, and hence, infrared spectroscopy is also useful in studying this interaction. Functional groups can be associated with characteristic IR absorption bands, which correspond to the fundamental vibrational modes of these functional groups [1]. In the past, dispersive instrumentation was used to obtain infrared spectra, but this approach has been almost superseded by sophisticated Fourier transform infrared (FTIR) spectroscopy. FTIR spectrometers have high signal to noise ratio, high optical throughput, and internal wavenumber calibration. Therefore, it is more advantageous as compared to dispersive instruments.

The basic components of an FTIR spectrometer are mainly an infrared source, Michelson interferometer, sample chamber, detector, amplifier, analog−to−digital converter and computer processor for performing Fourier transform of the signal [2].

The most commonly used interferometer in FTIR spectrometers is Michelson interferometer, which consists of a germanium coated KBr beam splitter, bisecting the

planes of a movable and a fixed mirror as shown in Fig. 2.1. When a collimated beam of radiation is passed through the beam splitter, half of the incident radiation is reflected to one of the mirrors while the other half is transmitted to the other mirror. The two beams after reflection from these mirrors return to the beam splitter and interfere. One beam travels a fixed length and the other path is constantly changing as its mirror moves. The signal from the detector is the result of these two interfering beams. It is called an interferogram [3] which has information about every infrared frequency which comes from the source. The interferogram is a signal produced as a function of the change of path length between the two beams introduced by moving mirror. The two domains of functions (distance and frequency) are interconvertible by the mathematical method of Fourier transformation. To obtain a frequency spectrum**,** the measured interferogram can be interpreted by a Fourier transformation which is performed by the computer. Since, all frequencies are being measured simultaneously; the Michelson interferometer produces fast measurements.

The typical experimental arrangement of FTIR spectrometer is shown in Fig. 2.1. For the IR spectroscopy, the Globar or Nernst glower source is commonly used. The normal detector for routine use is a pyroelectric device incorporating deuterium triglycine sulfate (DTGS) and, for more sensitivity, mercury cadmium telluride (MCT) can be used but it has to be cooled to liquid N_2 temperatures

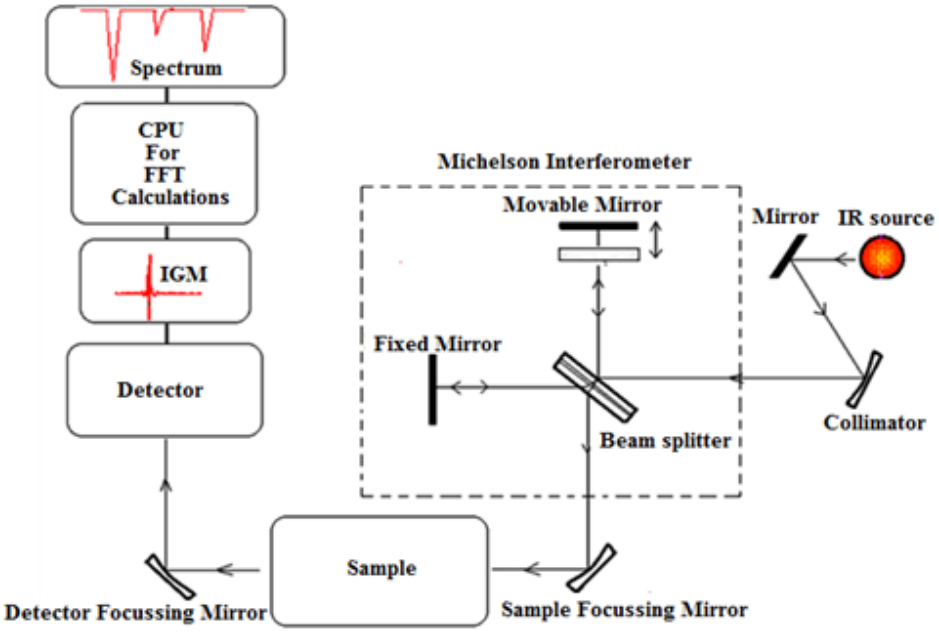

Fig. 2.1 Layout of FTIR spectrometer.

The radiation emerging from the source is passed to the sample through the interferometer before reaching a detector. On amplification of the signal, in which

high-frequency contributions have been eliminated by a filter, the data are converted to a digital form by an analog-to-digital converter and transferred to the computer for Fourier transformation. In this transformation, the intensity, $I(x)$, which is a function of optical path difference, is subjected to transform as a whole to give spectrum, $G(\bar{v})$, which is a function of the wavenumber. The integral used in Fourier transformations is given as follow:

$$F[I(x)] = G(\bar{v}) = \int_{-\infty}^{\infty} I(x) e^{-i2\pi\bar{v}x}\, dx \tag{2.1}$$

where, the interferogram, $I(x)$ is defined as

$$I(x) = \int_{-\infty}^{\infty} G(\bar{v})\ e^{-i2\pi\bar{v}x} dv \tag{2.2}$$

In practical, *x* does not go from -∞ to ∞. The maximum distance moved by the movable mirror has to be restricted to some finite distance, *L*. Therefore, a function, which is known as apodization function, is multiplied to interferogram. Some important apodization functions are boxcar, triangular, Happ−Genzel and Blackman−Harris functions. Different apodization functions are used for different purposes such as removing side lobes or minimizing smearing of the central absorption peak [4]. Boxcar apodization arises naturally due to finite mirror movement in a Michelson interferometer, and it multiplies collected interferogram data points by unity and is defined to be zero outside the range of mirror travel [5].

Some of the important advantages of FT-IR over the dispersive technique are Fellgett, Jacquinot and Connes advantages. All of the frequencies are measured simultaneously. This is referred as the Fellgett advantage. The FTIR measurements are made in few seconds rather than several minutes as in dispersive devices. The fast scans of the FTIR spectrum make able to record several scans for signal averaging in order to improve the signal-to-noise ratio of the measurement. The random measurement noise is drastically reduced to a desired level. The optical throughput of FTIR spectrometer is much higher because no slit is used in it which results in much lower noise levels. It is called Jacquinot advantage. The FTIR spectrometer is equipped with circular aperture of relatively lager dimension. The efficiency of the spectrometer is mainly due to this advantage. In addition to this, the detectors employed are more sensitive, therefore, sensitivity of the FT measurement is drastically improved.

The FTIR instrument is employed with a He-Ne laser for internal wavelength calibration. It is called Connes advantage. The position and movement of the movable mirror are controlled by He-Ne laser. The interferogram of the laser is used to control the sampling of the interferogram. The accuracy of the spectral frequencies is due to precise collection of the inteferogram signal triggered by the laser. The moving mirror is the only moving part in the interferometer, therefore, there is very little possibility of mechanical breakdown. All these advantages make measurements extremely accurate and reproducible. The sensitivity and accuracy of measurement as well as advanced software algorithms, have made the FTIR spectroscopy suitable for both quantitative and qualitative analysis.

2.1.1.1 Sample preparation

In the present study, KBr pellet technique has been used to record the FTIR spectra of the samples. In this technique, the sample is finely grinded with KBr in the ratio of 1:200. The mixture is then transformed into transparent pellets by subjecting about 6–8 metric ton pressure in a suitable die. The only precaution to be taken is to prevent the mixture from atmospheric moisture. The pellets are then placed in the FTIR spectrometer in a suitable holder and the IR beam is passed through it to get the spectrum.

2.1.2 Raman spectroscopy

In 1928, an Indian physicist, Chandrashekhara Venkata Raman discovered the phenomena based on inelastic scattering of light, known as the Raman effect, which explains the shift in the wavelength of a small fraction of radiation scattered by molecules from that of the incident beam [6]. Raman effect provides information about the structure, symmetry, electronic environment and bonding of the molecule. A molecular vibrational mode is Raman active when there is a change in polarizability during the vibration. The irradiation of a molecule with a monochromatic light always results in either elastic or inelastic scattering. The elastic or Rayleigh scattering results in no change in photon frequency. However, the inelastic scattering shifts photon frequency. Either the incident photon may lose or gain some amount of energy. The process in which the frequency of the scattered light is higher than that of incident light is known as anti-stokes Raman scattering, while the process in which the frequency of the scattered light is lower than that of the incident light is called as

stokes Raman scattering. The phenomenon of Raman scattering is shown in Fig. 2.2. In case of the vibrational Raman spectroscopy, Stokes bands involve the transitions from lower to higher energy vibrational levels and therefore, Stokes bands are more intense than anti-Stokes bands and these are measured in conventional Raman spectroscopy.

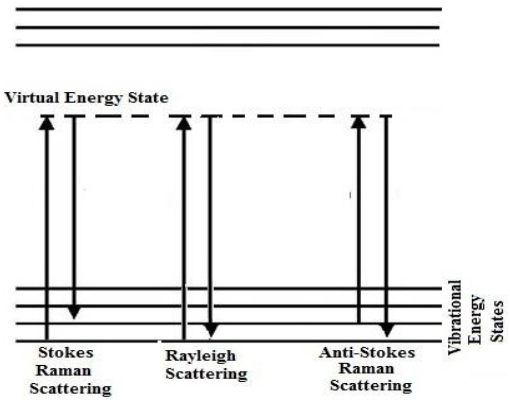

Fig. 2.2 Mechanism of Raman scattering.

Raman spectroscopy is a versatile method for analysis of a wide range of samples. It has resolved many limitations of other spectroscopic techniques. Numbers of papers describing the utility of Raman spectroscopy are available in the literature [7–12]. It is used for both qualitative and quantitative purposes. Qualitative analysis can be performed by measuring the frequency of scattered radiations while quantitative analysis can be performed by measuring the intensities of scattered radiations.

Raman spectrometers basically employ either dispersive or Fourier transform spectroscopic techniques to measure the spectra. The two techniques differ only in the way by which Raman scattering signal is detected and analyzed. Both these methods have some advantages over the other and the method that best suits the sample is preferred [13,14]. The frequent interference from fluorescence of either the target molecule or other components in the sample is reduced in FT-Raman technique using near–infrared excitation lasers. However, dispersive Raman spectrometers are low sensitive than FT-Raman spectrometers and overall loss of the signal occurs due to λ^{-4} dependence of the scattering process [15–17]. A Raman spectrometer is composed of excitation source, sample holder, optical system for sample illumination and collection of scattered light, monochromator or interferometery system and detector. The experimental arrangements for FT-Raman and dispersive spectrometers are shown in Fig. 2.3 (a) and (b).

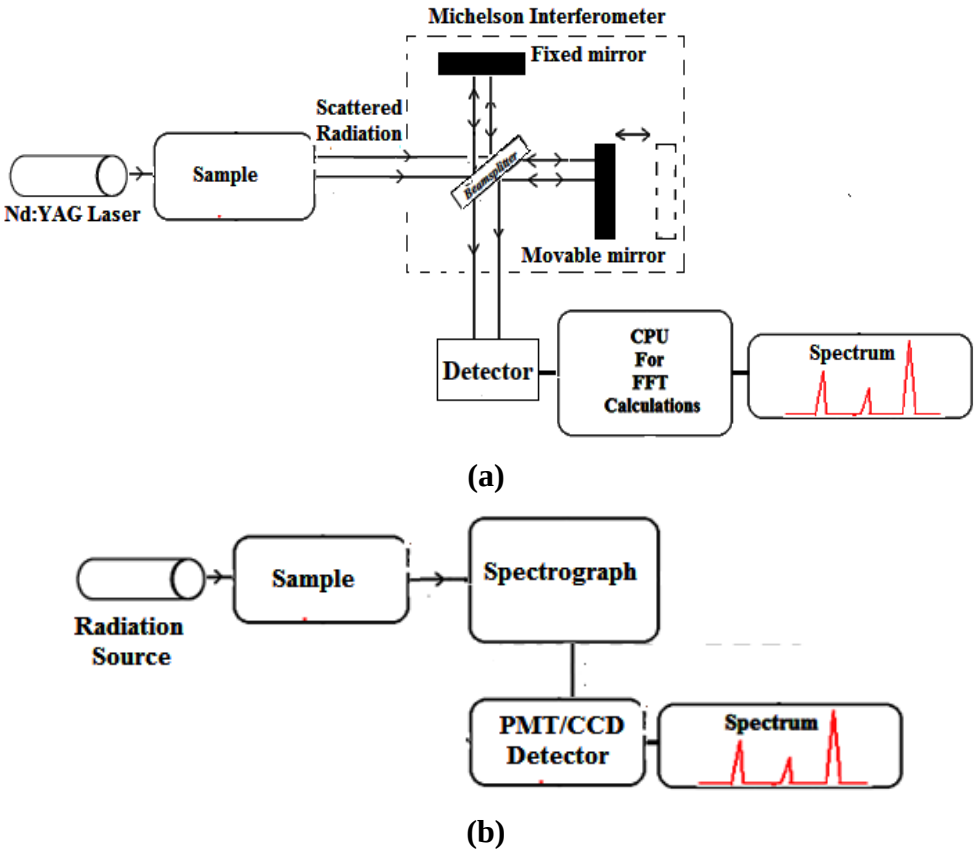

Fig. 2.3 Layout of **(a)** FT-Raman and **(b)** dispersive Raman spectrometer.

Since Raman scattering is a weak effect, the excitation source should be highly intense. The intensities of the Raman lines are related to the forth power of the frequency of the laser and the square of the polarizibility of the molecule. The UV radiation has higher frequency. It produces less fluorescence but it can degrade the sample. The choice of the laser depends on the situation. The laser sources like argon ion (488.0 and 514.5 nm), krypton ion (530.9 and 647.1 nm), He:Ne (632.8 nm), Nd:YAG (1064 nm and 532 nm) and diode laser (630 and 780 nm) are used as excitation sources. The laser power incident on the sample is selected in between 10 and 1000 mW. The laser may be continuous or quasi-continuous. Nd:YAG (1064 nm) laser source is generally preferred due to its lower fluorescent effect than visible wavelength lasers [18]. A severe limitation of Raman spectroscopy is the fluorescence phenomenon which is 10^7 times stronger than Raman scattering. A small amount of impurities can give strong fluorescence so that it is impossible to detect the Raman spectrum of the molecule of interest. To avoid masking of Raman scattering by fluorescence, NIR excitation is preferred, because there are very few electronic transitions in the NIR. The disadvantage of NIR excitation is that it reduces the Raman scattering intensity [19].

The 90º and 180º scattering geometries are used in collecting Raman scattering and both the arrangements are effective. In the 180º scattering system, the laser is delivered through the collection lens and the scattered light is collected back through same lens [20].

The Rayleigh scattering is avoided by using a notch filter in the interferometery system. The scattered light is collected with a low f-number lens. The single monochromator should not be used for the Raman measurement because stray light is not reduced to desired level in it. Therefore, double or triple monochromater is preferred. The commonly used double monochromator mounting is Czerny-Turner arrangement. The triple monochromators are suitable for the measurement of low frequency bands near Rayleigh line. The first monochromator mainly separates the frequency-shifted Raman scattering from the other radiation and the second monochromator increases the dispersion and separates the Raman peaks. Triple monochromators in additive mode have high angular dispersion and permit the recording of Raman spectra with very good resolution [19].

Detectors are important parts of Raman spectrometers due to the low intensity of Raman bands. In earlier days, the photographic plate was used as a detector to record the Raman spectra. Advances in the instrumentation and technology replaced this detector with more sensitive photomultipliers, image intensifiers and optical multichannel analyzers. These have greatly enhanced the detection sensitivity. Photomultiplier has good characteristics in the ultraviolet and visible spectral regions, hence they are the preferred detectors in a single channel dispersive Raman spectrometer. The sensitivity of photomultipliers is limited by their dark current which decreases with decreasing temperature. For routine Raman experiments, Peltier cooling is often sufficient. Instrumentation such as optical multichannel analyzers or charge-coupled device (CCD) arrays allow simultaneous recording of extended spectral ranges with sensitivities comparable to those of photomultipliers. Multichannel detection at the single photon level is achieved with a back-illuminated CCD. CCD's are characterized by a high dynamic range (≤100 dB), high quantum efficiency (90%), wide spectral range (350–900 nm) and low read-out noise (4-6 e^-).

Commercial Fourier Transform-Raman spectrometers (FT-Raman) were introduced in late 1980's. FT-Raman spectrometer uses a Michelson interferometer and continuous wave laser such as Nd–YAG. FT-Raman spectra are commonly measured in a 90° scattering geometry. Commercial systems use a Nd:YAG laser

(1.064 μm) with a near-infrared interferometer coupled to either a liquid nitrogen cooled germanium (Ge) or indium gallium arsenide (InGaAs) detector. Lasers with short pulses are not suitable for Raman spectrometer, because the detectors in Raman spectrometers are highly sensitive and they get saturation very easily.

In the FT-Raman spectrometer, the scattered radiation is focused on the entrance port of a conventional FTIR Spectrometer where the internal light source of absorption FTIR spectroscopy is removed. The analysis of the Raman spectrum is performed using Fourier transform technique. In a modern instrument, weak and broad but recognizable spectra can be obtained even with low power and low-cost lasers. Raman scattering using a Raman microscope with a laser pointer or He-Ne laser can be recorded.

In fact, all advantages of FTIR spectroscopy, as discussed in the above section, benefit the Raman analysis. In addition to the multiplex and throughput advantages, the higher wavenumber accuracy is obtained in the interferometric method. The FT-Raman technique references the measured frequencies to the accuracy of frequency of an internal He-Ne laser. Therefore, the absolute frequency can be determined to better than 0.01 cm^{-1} and the recorded band positions are limited by the collection parameters.

FT-Raman spectroscopy has provided a means of measuring the Raman spectrum of visible absorbers without masking by fluorescence. When using the 1064 nm line of a Nd:YAG laser as an excitation source, the Stokes shifted Raman spectrum occurs in the near infrared. The Raman frequencies in an FT-Raman spectrometer have Rayleigh and Tyndall radiation at laser frequency which is up to eight orders of magnitude more intense than the Raman scattering, hence it can cause saturation or even cause damage to the detectors. Hence, a filter for filtering out radiation at laser frequency is an essential component of an FT-Raman spectrometer. The best Rayleigh filter has a cut-off frequency closer to the exciting laser frequency. Rayleigh filters is the main limiting factor, preventing application of FT-Raman spectrometers in low frequency Raman spectroscopy [19].

2.1.3 UV–Vis spectroscopy

The absorption of electromagnetic radiation in the UV–Vis region causes a change in the electronic states of molecules. Molecules having electrons in the delocalised aromatic systems often absorb in the wavelength region 800–200 nm, resulting in

excitation of valence electrons from the ground electronic state to the excited electronic state. Ultraviolet spectra are measured by dissolving the sample in a solvent. The absorption is measured as a function of wavelength. The informations obtained from any absorption peak are wavelength of the peak maximum, denoted by λ max, and the intensity of the absorption. The intensity depends on Lambert's law, which states that absorbance of a material is directly proportional to the thickness (path length) and the fraction of the radiation absorbed is independent of the intensity of the radiation source, and Beer's law, which states that the absorption is proportional to the number of absorbing molecules. For a given ideal solution, there is a linear relationship between concentration and absorbance provided that the path length is kept constant; molar extinction coefficient (ε) is constant for each wavelength.

$$A = \varepsilon cl = \log_{10} \frac{I_o}{I} \tag{2.3}$$

where, *c* is the molar concentration and *l is* the path length in cm, I_o is the intensity of radiation before entering the sample and I is the intensity after leaving the sample [21,22]. The experimental layout of UV–Vis spectrophotometer is shown in Fig. 2.4.

The radiation sources are a deuterium lamp, which emits light in the UV region and a tungsten–halogen lamp for the visible region. After passing through a monochromator, the light is focused on two separate cuvettes inside the sample chamber. One of the cuvetts contains only the solvent and acts as a reference while the another one contains sample dissolved in the solvent. The commonly used detector is a photomultiplier tube (PMT). The light intensity measured by the detector is converted by it into an electrical signal and is plotted as a function of wavelength. However, for molecules, vibrational and rotational energy levels are superimposed on the electronic energy levels. Therefore, the electronic bands are broad as many transitions with different energies can occur. The broadening is even greater in solutions owing to solvent-solute interactions [23].

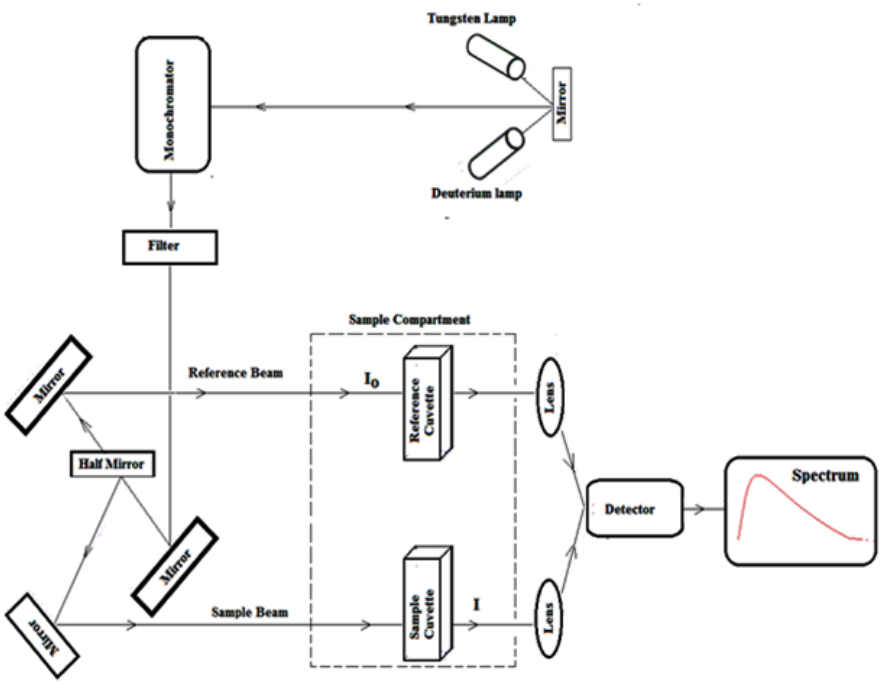

Fig. 2.4 Layout of UV–Vis Spectrophotometer.

2.2 Theoretical methods

The molecular simulation using the advanced quantum chemical methods is an exciting field of research in many disciplines like physics, chemistry, biology, biochemistry, biotechnology, etc. The primary focus of the quantum chemical calculations is the prediction of structures having minimum energy and other molecular properties. The calculations are performed taking different parameters into account which are based on the fundamental laws of physics. The *ab initio* treatments of polyatomic molecules consist of Hartree−Fock (HF) method, which excludes electron correlation, and post Hartree−Fock methods like Moller–Plesset perturbation (MPn), coupled-cluster (CC), multi−configuration self–consistence field (MCSCF) and configuration interaction (CI), which include electron correlation [24,25]. These, however, are the most computationally demanding and restrict the size of the molecules. These calculations are based upon the basic laws of quantum mechanics and exploit a variety of mathematical transformation and approximation techniques to solve the fundamental equations [26]. The density functional theory (DFT) methods take the effect of electron correlation into account by using exchange−correlation functionals and attempt to calculate the ground state electron density rather than molecular wave function and calculate the molecular energy functional. Presently, DFT is most popular and successful approach to compute properties of medium to

large sized molecular systems because of its high accuracy and relatively low computational cost. These theoretical calculations have gained popularity amongst the scientific community due to the advancement in theoretical models, computer hardwares and softwares.

2.2.1 Hartree–Fock method

Hartree and Fock proposed *ab initio* approach to solve the Schrodinger equation by invoking variational principle for many electron systems. The many-electron Schrodinger equation is broken into many simpler one-electron equations. Each one electron equation is solved to yield a single-electron wave function (called an orbital) and an energy (called an orbital energy). The orbital describes the behaviour of an electron in the net field of all the other electrons. The equations are solved using an iteration procedure that gives rise to self−consistence field (SCF) method which uses mean field, non−relativistic, Born−Oppenheimer and molecular orbital approximations to solve fundamental equation. According to Born−Oppenheimer approximation, the nuclei of the molecules are treated as stationary and produce a static potential field in which electrons are moving. HF method assumes that the electrons, which are moving in static potential, are not interacting to each other. In this method, the primary approximation (central field approximation) is that the Coulombic electron–electron repulsion is taken into account by integrating the repulsion term. This gives the average effect of the repulsion but not the explicit repulsion interaction.

Any problem in the electronic structure is solved by time dependent Schrodinger equation. However, in most cases, while dealing with atoms and molecules, time independent interactions are taken into account, which is given by

$$\hat{\mathrm{H}}\psi = E\psi \tag{2.4}$$

where, E is the electronic energy and ψ is the wave function, the Hamiltonian operator is given by [27].

$$\hat{\mathrm{H}} = -\frac{1}{2}\sum_{i}^{elec}\nabla_a^2 - \sum_{i}^{elec}\sum_{j}^{nucl}\frac{Z_A}{|\vec{R}_j - \vec{r}_i|} + \sum_{i}^{elec}\sum_{i'<i}^{elec}\frac{1}{|\vec{r}_i - \vec{r}_{i'}|} + \sum_{j}^{nucl}\sum_{j'<j}^{nucl}\frac{Z_A Z_{A'}}{|\vec{R}_j - \vec{R}_{j'}|} \tag{2.5}$$

where, 1st term is the kinetic energy operator, 2nd, 3rd and 4th terms represent all possible interactions (potential energies) between charged particles.

For a given system, equation (2.4) has many independent solutions with eigenfunctions ψ_k and eigenvalues E_k. ψ_k is always taken to be normalized and orthogonal i.e.

$$\int \psi_k^* \psi_l dx = \langle \psi_k | \psi_l \rangle = \delta_{kl} \tag{2.6}$$

δ_{kl}=1 for k=l and δ_{kl} =0 otherwise. The average of many measurements of energy is given by:

$$E[\psi] = \frac{\langle \psi | \hat{\mathrm{H}} | \psi \rangle}{\langle \psi | \psi \rangle} = \frac{\int \psi^* \hat{\mathrm{H}} \psi \, dx}{\int \psi^* \psi \, dx} \tag{2.7}$$

Since, each measurement gives one particular eigenvalue of $\hat{H}$, we have;

$$E[\psi] \geq E_0 \tag{2.8}$$

Equation (2.8) is the variational principle which states that the energy computed from a trial wavefunction ψ is always an upper bound to the true ground-state energy. Thus, one can use the iteration procedure for finding the set of coefficients that minimize the energy of the resultant wavefunction. The general idea is that the lower the energy, the better the trial wavefunction.

Molecular orbitals (MOs) can be written as linear combinations of pre−defined set of one−electron functions known as basis functions or basis sets. These basis functions are usually centred on the atomic nuclei and so resemblance to atomic orbitals. The wave function describing each molecular orbital can be expressed as follows:

$$\psi_i = \sum_{\mu=1}^{N} c_{\mu i} \phi_\mu \tag{2.9}$$

where, the coefficients $c_{\mu i}$ are known as the molecular orbital expansion coefficients and N is the number of basis functions. The function ϕ_μ refers to a trial basis function and thus ψ_i represents a trial MO. The ϕ_μ are also chosen to be normalized.

According to the Pauli exclusion principle, no two electrons can occupy the same spin orbital. Therefore, two electrons satisfying the antisymmetry principle can have same spatial orbital but must differ in spin functions. The antisymmetry is necessary due to the fermionic character of electrons. For a system having even number of electrons, restricted Hartree-Fock, (RHF) method is taken into

consideration. *N* orbitals ψ_i are compromised of *N/2* orbitals of the form $\phi_k(r)\alpha(\boldsymbol{s})$ and *N/2* orbitals of the form $\phi_k(r)\beta(\boldsymbol{s})$, where $\phi_k(r)$ represents the spatial orbital and $\alpha(\boldsymbol{s})$ and $\beta(\boldsymbol{s})$ are the spin functions [27]:

$$\Psi(HF) = \frac{1}{\sqrt{N!}}\begin{vmatrix} \phi_1\alpha(1) & \phi_1\beta(1) & \phi_2\alpha(1) & \phi_2\beta(1) & \cdots & \phi_{\frac{N}{2}}\alpha(1) & \phi_{\frac{N}{2}}\beta(1) \\ \phi_1\alpha(2) & \phi_1\beta(2) & \phi_2\alpha(2) & \psi_2\beta(2) & \cdots & \phi_{\frac{N}{2}}\alpha(2) & \phi_{\frac{N}{2}}\beta(2) \\ \vdots & \vdots & & & \vdots & \vdots & \vdots \\ \phi_1\alpha(N) & \phi\beta(N) & \phi_2\alpha(N) & \phi_2\beta(N) & \cdots & \phi_{\frac{N}{2}}\alpha(N) & \phi_{\frac{N}{2}}\beta(N) \end{vmatrix} \quad (2.10)$$

The expectation values of the energy form equation (2.7) are obtained by putting normalization integral $\langle\psi|\psi\rangle$ =1. It is expressed as

$$E_{HF} = \langle\psi_{HF}|\hat{\mathrm{H}}|\psi_{HF}\rangle = 2\sum_{K=1}^{N/2} H_k + \sum_{k,l=1}^{N/2} 2J_{kl} - K_{kl} \quad (2.11)$$

where, $H_k = \int \phi_k^*(r)\left[-\frac{1}{2}\nabla^2 + v(r)\right]\phi_k(r)dr$, J_{kl} and K_{kl} are the coulomb and exchange integrals and $\sum_{k,l=1}^{N/2} 2J_{kl} - K_{kl}$ is the electron electron repulsion energy. The Hartree-Fock equations are then given by

$$\hat{F}\phi_k(\boldsymbol{r}) = \sum_{l=1}^{\frac{N}{2}} \varepsilon_{kl}\,\phi_l(\boldsymbol{r}) \quad (2.12)$$

where, ε_{kl} is a matrix consisting of Lagrange multipliers.

2.2.2 Moller–Plesset perturbation theory

The Moller-Plesset (MP) perturbation theory was proposed in 1934. This theory provides a systematic approach to calculate the correlation energy of molecular systems. However, these calculations are not variational. Therefore, the results are not in general an upper-bound of the true ground state energy. The zero order (unpertubed) Hamiltionian $\hat{H}^{(0)}$ is defined as the sum of all the *N* one-electron Hartree-Fock Hamiltoninas ($\hat{H}_i^{HF}$) [28]:

$$\hat{H}^{(0)} = \sum_{i=1}^{N} \hat{H}_i^{HF} \quad (2.13)$$

The first-order perturbation $\hat{H}^{(1)}$ is then given by

$$\hat{H}^{(1)} = \hat{H} - \hat{H}^{(0)} \quad (2.14)$$

where, $\widehat{H}$ is the true molecular Hamiltonian (equation (2.5)). The HF energy associated with the normalized ground state wavefunction is written as

$$E_{HF} = \langle \psi^{HF} | \widehat{H} | \psi^{HF} \rangle = \langle \psi^{HF} | \widehat{H}^{(0)} | \psi^{HF} \rangle + \langle \psi^{HF} | \widehat{H}^{(1)} | \psi^{HF} \rangle \quad (2.15)$$

$$E_{HF} = E^{(0)} + E^{(1)} \quad (2.16)$$

where, $E^{(0)}$ is the zero order HF energy and $E^{(1)}$ is the first order HF energy. The first order correction to the ground state energy due to electron correlation in an electronic system is given by second order perturbation theory (MP2), which can be written as

$$E_0^{(2)} = \sum_{j \neq 0} \frac{\langle \psi_j^{HF} | \widehat{H}^{((1))} | \psi_0^{HF} \rangle \langle \psi_0^{HF} | \widehat{H}^{((1))} | \psi_j^{HF} \rangle}{E_0^{(0)} - E_j} \quad (2.17)$$

The Moller-Plesset calculation up to second order is called MP2 method, whereas higher order corrections are called as MP3, MP4 and so on [29–32]. These calculations are not applicable to excited states and are also to be used with a higher basis set for useful results [33]. Correlated models are, however, very useful for reliable thermodynamic information.

2.2.3 Density functional theory

Density functional theory (DFT) is an important quantum mechanical approach to calculate the properties of molecular systems by the inclusion of electron density, $\rho(\boldsymbol{r})$, where,

$$\rho(\boldsymbol{r}) = f(x, y, z) \quad (2.18)$$

Since, density is a function of wavefunction ψ (functional), the probability of finding an electron within a volume element dr in an N electron system with arbitrary spin is given by

$$\rho(\boldsymbol{r}) = N \int \dots \int |\psi(x_1, x_2, \dots, x_N|^2 \, dS_1 dx_2 .., .. dx_N \quad (2.19)$$

Here, the integral is solved over the spin coordinates of all electrons and overall but one of the spatial orbitals. The electron density is observable unlike the wavefunction and can be measured experimentally. Therefore, electron density is more attractive and effective in explaining the molecular properties. The ground state properties of a molecular system are functionals of the electron density and it is the basic of modern DFT. The concept was introduced by Hohenberg and Kohen in 1964 [34,35]. The

ground state energy of a molecule is at minimum if the density corresponds to the exact density of the ground state, however, the exact form of the energy functional is not known. Therefore, some approximations are needed. These approximations include the functional dealing with the kinetic, exchange and correlation energies of the system of electrons.

According to Hohenberg and Kohn, the ground state properties of a system can be calculated from the ground state density which in turn can be calculated using the variational method involving density only.

The ground state properties of an electronic system are a result of the position of the nuclei. If $\hat{V}_{ext}$ is the external potential due to the nuclei, the kinetic energy of the electrons, electron-electron interaction in the Hamiltonian and the electron density adjust themselves to give the possible minimum energy of the system. Hence, $\hat{V}_{ext}$ is the only variable term and is determined by ρ, which determines the number of electrons:

$$\int \rho(\boldsymbol{r})dr = N \tag{2.20}$$

Therefore, the total density replaces ψ, which describes ground state properties and state of the system. Hence, the energy can be respectively written as the sum of the kinetic energy of electrons, interaction energy between them and the energy corresponding to the external potential:

$$E[\rho] = T_{ee}[\rho] + V_{ee}[\rho] + V_{ext}[\rho] \tag{2.21}$$

For a trial density $\tilde{\rho}(r)$, such that $\tilde{\rho}(r) \geq 0$ and $\int \tilde{\rho}(r)dr = N$,

$$E_0 \leq E[\tilde{\rho}\,] \tag{2.22}$$

where, $E[\tilde{\rho}\,]$ is the energy functional. Each trial density $\tilde{\rho}$ defines a Hamiltonian $\tilde{\hat{\mathrm{H}}}_{el}$. From the Hamiltonian, the wavefunction $\tilde{\psi}$ for the ground state can be derived. This wavefunction will not be a ground state for the Hamiltonian $\hat{\mathrm{H}}_{el}$of the real system:

$$\langle\tilde{\psi}|\hat{\mathrm{H}}|\tilde{\psi}\rangle = E[\tilde{\rho}] \geq E[\rho_0] \equiv E_0 \tag{2.23}$$

where, $\rho_0(r)$ is the true ground state density of the real system. The condition of minimum energy functional is then given by:

$$\delta E[\rho(\boldsymbol{r})] = 0 \tag{2.24}$$

Although the Hohenberg Kohn method provides minimized energy of a system, the kinetic energy is not known with a satisfactory level of accuracy. Kohn and Sham proposed a method to determine the kinetic energy by combining wavefunctions and

the density approach. According to Kohn and Sham, the energy functional can be written as

$$E[\rho] = T_0[\rho] + \int [\hat{V}_{ext}(r) + \hat{V}_{el}(r)]\,\rho_r dr + E_{xc}[\rho] \tag{2.25}$$

where, $T_0[\rho]$ is the kinetic energy of electrons in a system which has the same density ρ as the real system (non interacting electrons); $E_{xc}[\rho]$ is the exchange-correlation energy; $\hat{V}_{el}(r)$ is the pure coulomb interaction between electrons given by equation

$$\hat{V}_{el}(\boldsymbol{r}) = \int \frac{\rho(r')}{|r' - r|} dr' \tag{2.26}$$

The exchange energy arises due to the antisymmetry of the wavefunction while correlation effects are because of the dynamic correlation in the motion of individual electrons [24]. The effective potential is then given by:

$$\hat{V}_{eff}(\boldsymbol{r}) = \hat{V}_{ext}(r) + \hat{V}_{el}(r) + \hat{V}_{xc}(r) \tag{2.27}$$

where, $\hat{V}_{ext}(r) = \sum_a \frac{-Za}{|Ra-r|}$ is the external potential, the potential reflected from the nuclei. The exchange correlation potential is defined as:

$$\hat{V}_{xc}(\boldsymbol{r}) = \frac{\delta E_{xc}[\rho(r)]}{\delta \rho(r)} \tag{2.28}$$

The Schrodinger equation for non interacting particles moving in external potential $\hat{V}_{eff}(\boldsymbol{r})$ is given as:

$$\left[\frac{-1}{2}\nabla_i^2 + \hat{V}_{eff}(r)\right] \emptyset_i^{KS}(r) = \in_i \emptyset_i(r)^{KS} \tag{2.29}$$

The Kohn Sham (KS) operator, $\frac{-1}{2}\nabla_i^2 + \hat{V}_{eff}(r)$, depends only upon r and the KS orbitals $(\emptyset_i(r)^{KS})$ are used to calculate the total density given by:

$$\rho(\boldsymbol{r}) = \sum_{i=1}^{N} \left|\emptyset_i^{KS}(r)\right|^2 \tag{2.30}$$

Although, KS DFT method gives good results for the medium to large molecular systems but has some drawbacks also because of the approximate functional [30]. The exchange correlation functionals include local spin density aproximation (LSDA), generalized gradient approximation functional (GGA), meta-GGA and hybrid functionals. The LSDA functionals assume slowly varying uniform electron density of the system. GGA approximation accounts for the non uniformity of the electron density and corrects the local density approximation through an additional density

gradient correction, which makes the functional more flexible. Some commonly used GGA exchange functionals are Perdew and Wang's (PW86, PW91) [36,37] and Becke's (B88) [38]. The meta-GGA functional modifies GGA by approximating the kinetic energy density. In the present thesis, Beck's 3 exchange and Lee-Yang-Par (B3LYP) hybrid correlation functional, the most widely used exchange−correlation functional within DFT calculations on molecules, has been used due to its accuracy. The B3LYP functional is defined as [39,40]

$$E_{xc}^{B3LYP} = (1 - a_0 - a_x)E_x^{LSDA} + a_0 E_x^{exact} + a_x E_x^{B88}$$
$$+(1 - a_c)E_c^{VWN} + a_c E_c^{LYP} \quad (2.31)$$

where, E_x^{exact} uses HF theory and a's are constants (empirical parameters).

2.2.4 Time dependent density functional theory

Despite its popularity, DFT being a static ground state theory, is not appropriate for handling time dependent phenomena or excited states. Time dependent density functional theory (TD-DFT) is one of the widely used simulation approach and extends the basic ideas of ground state DFT to the treatment of excitations or more general time dependant phenomenon. The time-dependant analogous of DFT (TD-DFT) was presented by Runge and Gross in 1984 [41] and the development of effective linear-response formalism by Casida leads to a rapid and efficient solution of TD-DFT equations for molecules [42]. TD-DFT shows that there is a one-to-one correspondence between time-dependent density $\rho(\boldsymbol{r}, t)$ and time-dependent potentials $v_{ext}(\boldsymbol{r}, t)$ for a given initial condition. By virtue of the one-to-one correspondence of potential and density, we can take the density of KS non-interacting electrons to be same as the interacting density of the original system. The time dependent KS electrons obey the time-dependent Schrodinger equation:

$$i\frac{\partial}{\partial t}\varphi_i(\boldsymbol{r}, t) = \hat{\mathrm{H}}_{KS}(\boldsymbol{r}, t)\varphi_i(\boldsymbol{r}, t) \quad (2.32)$$

where, $\hat{\mathrm{H}}_{KS} = -\frac{\nabla^2}{2} + v_{KS}[n](\boldsymbol{r}, t)$ is the Kohn-Sham Hamiltonian. The density $n(\boldsymbol{r}, t)$of the non-interacting system can be calculated from the Kohn-Sham orbitals:

$$n(\boldsymbol{r}, t) = \sum_{i}^{N} |\varphi_i(\boldsymbol{r}, t)|^2 \quad (2.33)$$

The time dependent Kohn-Sham potential is given by

$$v_{KS}[n](\boldsymbol{r},t) = v_{ext}(\boldsymbol{r},t) + v_{Hartree}[n](\boldsymbol{r},t) + v_{XC}[n](\boldsymbol{r},t) \quad (2.34)$$

The first term is the external potential, whereas the second accounts for the classical electrostatic interaction between the electrons. The third term, the v_{XC} potential has an essentially functional dependence on the density, includes all nontrivial many-body effects. The potential at time t and position $\boldsymbol{r}$ depends on the density at all other positions and all previous times. The final results depends upon the quality of approximation of v_{XC}, the only fundamental approximation in TD-DFT. v_{XC} is not only a functional of density, but it also depends on the initial Kohn-Sham determinant and on the initial many-body wave function, which is always neglected for practical reasons. Explicit density functionals, like the adiabatic LDA, only retain the density dependence [43].

2.2.5 Basis set

Basis sets constitute an essential component of the quantum chemical calculations to describe the molecular electronic structure. They provide a best mathematical description of the unknown molecular orbitals with a minimum possible computational cost. A large number of basis sets have been proposed over the years. The general expression for a basis function is given by

$$Basis\ function = N \times (e^{-\alpha r}) \quad (2.35)$$

where, N is the normalization constant, α is the orbital exponent and r is the distance from origin where the nucleus is located. It was John C. Slater who first turned to orbital computation using basis sets. These basis sets are known as Slater type orbitals (STOs). The STOs are defined as

$$\phi_1(\alpha, n, l, m; r, \theta, \phi) = Nr^{n-1}e^{-\alpha r}Y_{l,m}(\theta, \phi) \quad (2.36)$$

where, r, θ, ϕ are spherical coordinates, $Y_{l,m}$ is the angular momentum part which describes the shape and n, l, m are quantum numbers.

In 1950, Boys suggested Gaussian type functions (GTOs), which contain the exponential $e^{-\beta r^2}$, rather than $e^{-\alpha r}$ of the STOs and are easy to calculate. However, they neither represent the electron density nor the STOs. Therefore, each basis function consists of linear combination of several GTOs with fixed coefficients. GTO(3G) function can be defend as

$$GTO(3G) = C_1e^{-\alpha_1 r^2} + C_2e^{-\alpha_2 r^2} + C_3e^{-\alpha_3 r^2} \quad (2.37)$$

where, the three values of C and α are fixed and that number is included in the designation. The difference between STOs and GTOs is that the pre-exponential factor r^{n-1} in STO function is dropped in the GTO function, which restricts single Gaussian primitives for each principal quantum level. The exponential$r$factor in GTO is squared and the angular momentum factor is made into a simple function of Cartesian coordinates.

Minimal basis sets are represented in the form STO-nG, where, n denotes the number of primitive GTOs (G) used to approximate one STO for each inner and valence shell. They include STO-3G, STO-4G, STO-6G and the polarized version of STO-3G (STO-3G*). The individual GTOs are called primitive orbitals. A group of several GTOs form contracted Gaussian functions. STO-3G consists of three primitive Gaussians in each basis function.

Split valence basis sets include 3-21G, 3-21G* (polarized), 3-21+G (diffuse), 3-21+G* (polarized and diffuse), 6-31G, 6-31G*, 6-31+G*, 6-31G(3df,3pd), 6-311G, 6-311G*, 6-311+G* etc. These basis sets use one function for orbitals that are not in the valence shell and two functions for those in the valence shell. 3-21G is the smallest split valence basis set, which uses three primitive expansion for the 1s orbital and splits the valence orbitals into a two basis function. The inner function is a contraction of two Gaussians and the outer function is a single Gaussian. The double zeta basis set, considered as a general split valence basis set, uses two basis functions for each atomic orbital and each basis function is a contraction of small set of primitives. The triple zeta basis set uses three basis functions [44–46].

The 6-311G basis set is having triple zeta quality in the valence part and only minimal in the core. The flexibility of this basis set in the valence region of the molecule is increased by adding polarization functions. These functions have a set of Gaussian functions one unit higher in angular momentum than the Gaussian functions present in the ground state of the atom. The polarization functions are denoted by single (*) or double (**) asterisk or by (d,p). A single * or d denotes that polarization has been taken into account in the non-hydrogen atoms, whereas, ** or (d,p) represents that both hydrogen and non-hydrogen atoms are taken into account.

To account for the electron density over a large region for an atom in an anion, excited or Rydberg states and lone pair of electrons, diffuse functions are usually preferred. These are represented by + or ++, where + denotes the sp-type

diffuse basis functions added to non-hydrogen atoms and ++ indicates the consideration of one set of sp- and s-type diffuse functions to non-hydrogen and hydrogen atoms respectively.

2.2.6 Geometry optimization

The optimization of geometry plays an important role in the quantum chemical studies concerned with the structure determination or reactivity of molecules. The location of the atoms specify the structure of a molecule. For a given structure and electronic state, a molecule has a specific energy. By virtue of Born−Oppenheimer, the energy of a molecule can be described as a function of fixed nuclear positions. The variation of energy as function of the structure of a molecule is given by potential energy surface (PES),which can be visualized as a hilly landscape where the minimum energy position represents the equilibrium structure. The transition state structure is also represented in this PES. The procedure of locating stationery points (minima or maxima) on the PES for calculating geometry and energy of a molecule is called as geometry optimization. The efficient methods to find a local minimum require a repeated calculation of U (molecular electronic energy including inter-nuclear repulsions) and its gradient (3N-6 partial derivatives) [47]. For a structure to be characterized as minimum, the gradient must be zero and all the eigen values of the Hessian (matrix of second derivatives of energy, also known as Force constant matrix) corresponding to molecular vibrations must be positive. A transition state has a zero gradient and a Hessian that has only one negative eigen value (imaginary frequency). The performance of any geometry optimization can be improved by choosing a good coordinate system. The presence of very stiff and flexible coordinates, strong coupling between coordinates and other neighbouring coordinates and anharmonicity can slow down an optimization process [47]. Cartesian coordinates are the most universal and least ambiguous. However, they do not reflect the chemical structure and bonding of a molecule. The x, y and z coordinates are also coupled to each other and the surrounding coordinates of the atoms. Therefore, they are not well suited in optimization. Being more descriptive of the molecular structure, internal coordinates such as bond lengths and valence angles are however useful for optimization of the geometry. The coupling between stretches, bends and torsions are usually much smaller than in Cartesian coordinates. The combination of all bonds, angles and torsions (primitive redundant coordinate system) represent the intrinsic

connectivity and flexibility of cyclic molecules. However, such a coordinate system leads to sacking of geometrical parameters for the cyclic ones. Therefore, certain combinations of redundant internals need to be constrained during optimization [48–50].

2.2.7 Vibrational frequency calculations

The interpretation and correct assignment of the vibrational spectra of larger polyatomic molecules is virtually impossible without quantum-mechanical calculations. The computations of the vibrational frequencies are also essential to classify a stationery point as a local minimum or an nth order saddle point on the PES [30]. The vibrational frequencies are computed analytically from the optimized structure of a molecule by evaluating the Hessian or force constant matrix. The set containing *3N* linear equations in *3N* unknowns is solved:

$$\sum_{j=1}^{3N}\left(F_{ij}-\delta_{ij}\lambda_k\right)l_{jk}=0, \qquad i=1,2,3,\ldots,3N \tag{2.38}$$

where, δ_{ij} is the Kronecker delta, l_{jk} and λ_k are unknown parameters. F_{ij} is the mass weighted force constant matrix. For a nontrivial solution, the determinant of equation (2.36), which is of order *3N*, must be zero:

$$\det\ (F_{ij}-\delta_{\mathrm{ij}}\lambda_k)=0 \tag{2.39}$$

This determinant can be expended in polynomial form whose highest power of λ_k is λ_k^{3N} with *3N* roots for λ_k. The vibrational harmonic frequencies are obtained from relation:

$$\nu_k=\lambda_k^{\frac{1}{2}}/2\pi \tag{2.40}$$

The vibrational transitions in which the vibrational quantum number ν_k goes from 0 to 1 with no change in other quantum numbers are called the fundamental frequencies. These fundamental frequencies incorporate anharmonic corrections and are generally smaller than the harmonic frequencies. In order to account for the anharmonicity, effective corrections using empirical scaling factors are reported at various levels of theory, although they are not appropriate for all vibrational modes [51–58]. The overtone and combination bands are also not predicted using harmonic approximation. Therefore, to overcome these limitations of harmonic approximation, several anharmonic approaches have been proposed to account for the anharmonicity.

Among them, the vibrational self-consistent field (VSCF) theory and second order perturbative approaches like the vibrational second-order perturbation (VPT2) level of theory and second order perturbation corrected VSCF theory (VSCF–PT2, also referred to as correlation corrected VSCF (CC-VSCF) provide significant accuracy [59–65].

2.2.7.1 Second order perturbative approach

The second order perturbative (PT2) theory is very effective to study the anharmonic features of a polyatomic molecule of medium dimensions. The PT2 approach uses the quadratic, cubic and semi diagonal quartic force constants, effectively computed by a finite difference approach which scales linearly with the number of normal modes in the molecular system. The PT2 approximation can provide results more closer to the experimental data than their variational counter parts. However, the accuracy and efficiency of PT2 approach are affected by the vibrations involving high anharmonicity [66]. The vibrational second order perturbation theory (VPT2) has been recently implemented by Barone [67,68] in Gaussian package of programs [69]. One of the main advantages of the VPT2 approach is its cost efficiency to compute the more accurate vibrational anharmonic molecular spectra [68]. The choice of coordinate system like rectilinear coordinates fail to define the large amplitude vibrations in PT2 approach while it is appropriate method of choice for semi-rigid molecules. It nearly distorts for highly anharmonic and floppy molecules like peptides and proteins.

The vibrational energies of the states of interest of a system with N internal degrees of freedom are given by VPT2 approach as [67,68],

$$Fundamentals: \nu_i = \omega_i + 2x_{ii} + \frac{1}{2}\sum_{j\neq i} x_{ij} \tag{2.41}$$

$$Overtones: [2\nu_i] = 2\omega_i + 6x_{ii} + \textstyle\sum_{j\neq i} x_{ij} = 2\nu_i + 2x_{ii} \tag{2.42}$$

$$Combinations: [\nu_i\ \nu_j] = \omega_i + \omega_j + 2x_{ii} + 2x_{jj} + 2x_{ij} + \tfrac{1}{2}\textstyle\sum_{l\neq i,j}(x_{il} + x_{jl}) = \nu_i + \nu_j + x_{ij} \tag{2.43}$$

where, ω_i is the harmonic frequency of the i^{th} normal mode of vibration and x_{ij} is a square matrix of real anharmonic constants. The constant, x_{ii} characterizes anharmonicity of the given vibration; x_{ij} characterizes coupling between different

normal modes resulting from anharmonicity and are determined from cubic and quartic force constants.

2.2.7.2 Vibrational self−consistent field approach

The VSCF method is equivalent to the Hartree method used for many electron systems. The method, developed by Bowman, Carney, Cohen, Gerber and Ratner in late 1970s, is employed to account for the anharmonicity in molecules [70–73]. In this approximation, each vibrational mode is characterized by moving in the mean field of the rest of vibrational motions and the wavefunctions corresponding to different vibrational modes are determined using a self-consistent method. The total vibrational wavefunction is then written as a product of each normal mode wavefunctions. This method is equivalent to Hartree method for many electron systems and has been successfully used for small to medium sized molecules [74–78]. The major challenge for this approximation is the calculation of multidimensional potentials which depend on its typical mathematical form [79]. The VSCF potential is given by the adding one-mode, two-mode, three-mode terms and so on in mass weighted normal coordinate Q [79]:

$$V(Q_1 \dots,..Q_N) = \sum_{i=1}^{N} V_i^{diag}(Q_i) + \sum_{j}^{N}\sum_{i>j}^{N} V_{ij}^{2Coup}(Q_i, Q_j) + \sum_{k=1}^{N}\sum_{j>k}^{N}\sum_{i>j}^{N} V_{ij}^{3Coup}(Q_i, Q_j, Q_k) + \cdots \quad (2.44)$$

where, the first term represents the harmonic potential and the intrinsic anharmonicity of the potential function along the normal coordinates (diagonal approximation); the second term consists of pair-wise coupling between different normal modes, etc. The VSCF energy is then given by the self consistency approach as:

$$E_n^{VSCF} = \sum_{j=1}^{N} \varepsilon_j^{(n)} - (N-1)\langle \prod_{j=1}^{N} \psi_j^{(n)}(Q_j) | V(Q_1, \dots., Q_N) | \prod_{j=1}^{N} \psi_j^{(n)}(Q_j) \rangle \quad (2.45)$$

where, first term is the sum of all individual mode energies and the other terms accounts for the double counting of the interactions in the energy calculation. The accuracy of the VSCF approximation depends strongly on the choice of coordinates which can best reproduce the mutual separability for VSCF approximation [66]. The normal coordinate system often fails for soft torsional motions. The curvilinear

internal coordinates offer a good accuracy over the normal coordinates representation of VSCF. The second order perturbation corrected VSCF, PT2-VSCF (CC–VSCF), an important variant of VSCF, was introduced by Gerber and co-workers that improves the VSCF energies, keeping the computational cost in control for relatively large molecules. The total energy for the CC−VSCF approximation is given by:

$$E_n^{cc-VSCF} = E_n^{VSCF} + \sum_{m \neq n} \frac{\left| \langle \prod_{j=1}^{N} \psi_j^{(n)}(Q_j) \, | \Delta V | \, \prod_{j=1}^{N} \psi_j^{(m)}(Q_j) \rangle \right|^2}{E_n^{(0)} - E_m^{(0)}} \tag{2.46}$$

where,

$$\Delta V = V(Q_1, \ldots, Q_N) - \sum_{i=1}^{N} \overline{V_i^{(n)}}(Q_i) \tag{2.47}$$

where, $\overline{V_i^{(n)}}(Q_i)$ is the effective potential for mode i corresponding to $Q_{i,}$ ΔV is the difference between the correct Hamiltonian and VSCF one (perturbation) which must be small.

2.2.7.3 Quartic force field potential and anharmonic mode-mode coupling strength

The potential energy surface of a molecule consisting of N atoms is given by Taylor expansion as [80].

$$V(Q) = V_0 + \frac{1}{2}\sum_{i=1}^{f} h_i \, Q_i^2 + \frac{1}{6}\sum_{ijk}^{f} t_{ijk} \, Q_i Q_j Q_k + \frac{1}{24}\sum_{ijk}^{f} U_{ijkl} \, Q_i Q_j Q_k Q_l \tag{2.48}$$

where, V_0, h_i, t_{ijk} and U_{ijkl} denote the potential energy and its second, third and fourth order derivatives respectively and Q is the normal coordinate at the equilibrium structure. The third and fourth order energy derivatives can be obtained through numerical differentiation, while the higher order terms are neglected. Yagi and et. al. [80] developed a method to determine the expansion coefficient in the above equation energy derivatives calculated by an *ab initio* electronic structure method (least square fit method) at the equilibrium structure. In the two mode coupling representation of the quartic force field (2MR-QFF), which can be constructed with less computational effort than direct VSCF calculations, $V(Q)$ can be written as:

$$V_{QFF}^{(2)} = V_{QFF}^{(1)} + \sum_{i\neq j}^{f}\left[\frac{1}{2}t_{ijj}Q_jQ_j^2 + \frac{1}{6}U_{ijjj}Q_iQ_j^3\right] + \frac{1}{4}\sum_{i<j}^{f}U_{iijj}\,Q_i^2Q_j^2 \tag{2.49}$$

where,

$$V_{QFF}^{(1)} = V_0 + \sum_{i=1}^{f}\left[\frac{1}{2}h_iQ_i^2 + \frac{1}{6}t_{iii}Q_i^3\right] + \frac{1}{24}\sum_{i<j}^{f}U_{iiii}\,Q_i^4 \tag{2.50}$$

Similarly n-mode coupling representation quartic force field (nMR-QFF) can be determined from equation (2.46).

Anharmonic interactions are of two types: (1) intrinsic anharmonicity of the mode and (2) anharmonic mode-mode coupling. Therefore, the potential function, $V(Q_1,\ldots.,Q_N)$, in the 2MR-QFF approximation can be written as described in equation (2.42) upto two terms and neglecting the higher order terms. The contribution of the intrinsic anharmonicity in a mode is given by [81]

$$\Delta E_{daigonal} = \nu_{diagonal} - \nu_{harmonic} \tag{2.51}$$

The contribution of anharmonic mode pair coupling is given by

$$\Delta E_{Coup} = \nu_{CC-VSCF} - \nu_{daignol} \tag{2.52}$$

where, ν is the frequency. The detection of the mode coupling strengths is important in solving the vibrational Schrodinger equation and in generating a PES. The mode coupling strengths based on QFF coefficients can be potentially used to detect the strong coupling and discard terms that need not to be computed in generating a PES. The mode coupling strength based on 2MR-QFF for the ground state is given by

$$\eta_{iijj}^{(1)} = C_{iijj}\langle 0|Q_i^2Q_j^2|0\rangle = C_{iijj}\left(\frac{\hbar}{2\omega_i}\right)\left(\frac{\hbar}{2\omega_j}\right) \tag{2.53}$$

The coefficient C_{iijj} is obtained by numerical differentiations of the analytical Hessian.

References

[1]. C. Berthomieu, R. Hienerwadel, Photosynth. Res. 101 (2009) 157–170.

[2]. B.H. Stuart, Infrared Spectroscopy: Fundamentals and Applications, John Wiley & Sons, England, 2004.

[3]. B.H. Stuart, Infrared Spectroscopy of Biological Applications: An Overview, Encyclopedia of Analytical Chemistry, John Wiley & Sons, Ltd. 2012.

[4]. P.R. Griffiths, J.A. De Haseth, Fourier Transform Infrared Spectrometry, John Wiley & Sons, New York, 1986.

[5]. R.S. Brettzlaff, T.B. Bahder, Rev. Phys. Appl. 21 (1986) 833–844.

[6]. C.V. Raman, K.S. Krishnan, Nature 121 (1928) 501–502.

[7]. W. Kiefer, V. Pfeufer, P. Vogt, Spectroscopy 27 (2012) 28–35.

[8]. W. Kiefer, J. Raman. Spectrosc. 38 (2007) 1538–1553.

[9]. W. Kiefer, J. Raman. Spectrosc. 39 (2008) 1710–1725.

[10]. W. Kiefer, J. Raman. Spectrosc. 40 (2009) 1766–1779.

[11]. J. Popp, W. Kiefer, Encyclopedia of Analytical Chemistry, John Wiley & Sons Ltd, Chichester, 2000.

[12]. G.S. Bumbrah, R.M. Sharma, Egypt. J. Forensic Sci. (2015), http://dx.doi.org/10.1016/j.ejfs.2015.06.001

[13]. Y. Wang, R.L. McCreery, Anal. Chem. 61 (1989) 2647–2651.

[14]. R.S. Dass, Y.K. Agarwal, Vib. Spectrosc. 57 (2011) 163–176.

[15]. P. Hendra, C. Jones, G. Warnes, Fourier Transform Raman Spectroscopy: Instrumentation and Chemical Applications, Ellis Horwood Ltd, 1991.

[16]. D.B. Chase, J.F. Rabolt, Fourier Transform Raman Spectroscopy: From Concept to Experiment, Academic Press, New York, 1994.

[17]. I.R. Lewis, H.G.M. Edwards, Handbook of Raman Spectroscopy: From the Research Laboratory to the Process Line, Marcel Dekker, Inc, 2001.

[18]. J.R. Ferraro, K. Nakamoto, Introductory Raman Spectroscopy, 2nd edition, Academic Press, Boston, 1994.

[19]. G. Gauglitz, T. Vo-Dinh, Handbook of Spectroscopy, Wiley-VCH Verlag GmbH & Co. KGaA, Weinheim, 2003.

[20]. E. Smith, G. Dent. Modern Raman Spectroscopy: A Practical Approach, John Wiley & Sons, Ltd. 2005.

[21]. S.L. Upstone, Ultraviolet/Visible Light Absorption Spectrophotometry in Clinical Chemistry, Encyclopedia of Analytical Chemistry, John Wiley & Sons, Ltd. Chichester, 2000.

[22]. T. Owen, Fundamentals of UV-Vis Spectroscopy, Hewlett-Packard Company, Germany, 1996.

[23]. D. Whittaker, Interpreting Organic Spectra, The Royal Society of Chemistry, 2000.

[24]. C. Moller, M.S. Plesset, Phys. Rev. 46 (1934) 618−622.

[25]. J.A. Pople, M.H. Gordon, K. Raghavachari, J. Chem. Phys. 87 (1987) 5968−5975.

[26]. J.B. Foresman, A. Frisch, Exploring Chemistry with Electronic Structure Methods, 2nd edition, Gaussian, Inc, Pittsburgh, 1996.

[27]. R.G. Parr, W. Yang, Density-Functional Theory of Atoms and Molecules, Oxford University Press, New York, 1989.

[28]. M. Mueller, Fundamentals of Quantum Chemistry, Kluwer Academic Publishers, New York, 2002.

[29]. P. Atkins, R. Friedman, Molecular Quantum Mechanics, 4th edition, Oxford University Press Inc., New York, 2005.

[30]. I.N. Levine, Quantum Chemistry, 6th edition, PHI Learning Private Ltd., New Delhi, 2010.

[31]. C.J. Cramer, Essentials of Computational Chemistry: Theories and Models, 2nd edition, John Wiley & Sons, Ltd., England, 2004.

[32]. H.B. Schlegel, J. Comp. Chem. 3 (1982) 214−218.

[33]. K.I. Ramachandran, G. Deepa, K. Namboori, Computational Chemistry and Molecular Modelling: Principles and Applications, Springer, Verlag Berlin Heidelberg, 2008.

[34]. P. Hohenberg, W. Kohn, Phys. Rev. B 136 (1964) 864−871.

[35]. W. Kohn, Rev. Mod. Phys. 71 (1999) 1253−1266.

[36]. J.P. Perdew, J.A. Chevary, S.H. Vosko, K.A. Jackson, M.R. Pederson, D.J. Singh, C. Fiolhais, Phys. Rev. B 46 (1992) 6671−6687.

[37]. J.P. Perdew, W. Yue, Phys. Rev. B 33 (1986) 8800−8802.

[38]. A.D. Becke, Phys. Rev. A 38 (1988) 3098−3100.

[39]. C. Lee, W. Yang, R.G. Parr, Phys. Rev. B 37 (1988) 785−789.

[40]. A.D. Becke, J. Chem. Phys. 98 (1993) 5648−5652.

[41]. E. Runge, E.K.U. Gross, Phys. Rev. Lett. 52 (1984) 997–1000.

[42]. M.E. Casida, Recent Advances in Density Functional Methods, World Scientific, Singapore, 1995.

[43]. M.A.L. Marques, E.K.U. Gross, Annu. Rev. Phys. Chem. 55 (2004) 427–455.

[44]. R. Poirier, R. Kari, I.G. Csizmadia, Handbook of Gaussian Basis Sets, Elsevier, New York, 2007.

[45]. T.H. Dunning, Jr., J. Chem. Phys. 90 (1989) 1007−1023.

[46]. D.E. Woon, T.H. Dunning Jr., J. Chem. Phys. 98 (1993) 1358−1371.

[47]. H.B. Schlegel, WIREs Comput. Mol. Sci. 1 (2011) 790–809.

[48]. P. Pulay, G. Fogarasi, J. Chem. Phys. 96 (1992) 2856–2860.

[49]. J. Baker, A. Kessi B. Delley, J. Chem. Phys. 105 (1996) 192–212.

[50]. O. Farkas, H.B. Schlegel, J. Chem. Phys. 109 (1998) 7100–7104.

[51]. M.P Andersson, P.J. Uvdal, Phys. Chem. A 109 (2005) 2937−2941.

[52]. J.P. Merrick, D. Moran, L.J. Radom, Phys. Chem. A 111 (2007) 11683−11700.

[53]. Y. Tantirungrotechai, K. Phanasant, S. Roddecha, P. Surawatanawong, V. Sutthikhum, J. Limtrakul, J. Mol. Struct. (Theochem) 760 (2006) 189−192.

[54]. M.W. Wong, Chem. Phys. Lett. 256 (1996) 391−399.

[55]. D.J. Defrees, A.D. Mclean, J. Chem. Phys. 82 (1985) 333−341.

[56]. J.A. Pople, A.P. Scott, M.W. Wong, L. Radom, Isr. J. Chem. 33 (1993) 345−350.

[57]. A.P. Scott, L.J. Radom, Phys. Chem. 100 (1996) 16502−16513.

[58]. G. Rauhut, P. Pulay, J. Phys. Chem. 99 (1995) 3093−3100.

[59]. V. Barone, J. Chem. Phys. 122 (2005) 014108−014118.

[60]. J. M. Bowman, J. Chem. Phys. 68 (1978) 608–610.

[61]. G.D. Carney, L.L. Sprandel, C.W. Kern, Adv. Chem. Phys. 37 (1978) 305–379.

[62]. M. Cohen, S. Greita, R.D. McEarchran, Chem. Phys. Lett. 60 (1979) 445–450.

[63]. R.B. Gerber, M.A. Ratner, Chem. Phys. Lett. 68 (1979) 195–198.

[64]. L.S. Norris, M.A. Ratner, A.E. Roitberg, R.B. Gerber, J. Chem. Phys. 105 (1996) 11261–11267.

[65]. J.O. Jung, R. B. Gerber, J. Chem. Phys. 105 (1996) 10682–10690.

[66]. T. K. Roy, R. B. Gerber, Phys. Chem. Chem. Phys. 15 (2013) 9468−9492.

[67]. V. Barone, J. Chem. Phys. 122 (2005) 014108−014118.

[68]. V. Barone, M. Biszysko, J. Bloino, Phys. Chem. Chem. Phys.16 (2014) 1759–1787.

[69]. M.J. Frisch, G.W. Trucks, H.B. Schlegel, G.E. Scuseria, M.A. Robb et. al., Gaussian 09, Revision D.01, Gaussian, Inc., Wallingford CT, 2009.

[70]. J. M. Bowman, J. Chem. Phys. 68 (1978) 608–610.

[71]. G.D. Carney, L.L. Sprandel, C.W. Kern, Adv. Chem. Phys. 37 (1978) 305–379.

[72]. M. Cohen, S. Greita, R.D. McEarchran, Chem. Phys. Lett. 60 (1979) 445–450.

[73]. R.B. Gerber, M.A. Ratner, Chem. Phys. Lett. 68 (1979) 195–198.

[74]. T.K. Roy, T. Carrington Jr., R. B. Gerber, J. Phys. Chem. A, 118 (2014) 6730–6739.

[75]. K. Meng, J. Wang, Phys. Chem. Chem. Phys. 13 (2011) 2001–2013.

[76]. B. Brauer, R.B. Gerber, M. Kabelac, P. Hobza, J.M. Bakker, A.G.A. Riziq, M.S. de Vries, J. Phys. Chem. A, 109 (2005) 6974–6984.

[77]. L. Pele, R. B. Gerber, J. Chem. Phys. 128, (208) 165105–165115.

[78]. R. Knaanie, J. Sebek, J. Kalinowski, R. B. Gerber, Spectrochim. Acta A 119 (2014) 2–11.

[79]. T.K. Roy, R.Sharma, R. B. Gerber, Phys. Chem. Chem. Phys. 18 (2016) 1607–1614.

[80]. K. Yagi, T. Taketsuga, K. Hirao, M.S. Gordon, J. Chem. Phys. 113 (2005) 1005–1017.

[81]. Y. Miller, G.M. Chaban, R.B. Gerber, J. Phys. Chem. A 109 (2005) 6565–6574.